Progress In Electromagnetics Research, Vol. 142, 321–332, 2013

A SOLAR CELL STACKED SLOT-LOADED SUSPENDED MICROSTRIP PATCH ANTENNA WITH MULTIBAND RESONANCE CHARACTERISTICS FOR WLAN AND WiMAX SYSTEMS

Okan Yurduseven*, David Smith, Nicola Pearsall, and Ian Forbes

Faculty of Engineering and Environment, Northumbria University, Newcastle Upon Tyne, NE1 8ST, United Kingdom

Abstract—In this paper, a novel self-complementary shaped multiple-L slot loaded suspended microstrip patch antenna stacked with a polycrystalline silicon (poly-Si) solar cell is presented for 2.4/5.2 GHz band WLAN and 2.5/3.3/5.8 GHz band WiMAX networks. While the proposed self-complementary shaped multiple-L slot loaded suspended patch enables the propagation of multiple TM_{mn} modes to be present, the poly-Si solar cell works as an RF parasitic patch element in addition to its photovoltaic function. The proposed stacked solar antenna combination topology enables the radiating patch to be easily modified by slot-loading to achieve multiband resonance characteristics and the poly-Si solar cell to operate without being shaded by any RF components of the antenna ensuring an optimum solar operation performance.

1. INTRODUCTION

Solar powered communication systems have received considerable attention due to their advantage of being able to operate without the necessity of an electric grid connection which becomes a significant challenge when it comes to powering communication systems in places where an electric grid is not available. In order to address this challenge, the use of photovoltaics in communication systems has recently been the subject of much research. In the literature, two types of photovoltaics-antenna integration techniques have been demonstrated involving the autonomous integration of solar cells and

Received 15 August 2013, Accepted 28 August 2013, Scheduled 5 September 2013

* Corresponding author: Okan Yurduseven (okan.yurduseven@northumbria.ac.uk).

microwave antennas [1] and the full integration of these two elements in a self-powered communication system [2–8], respectively. The first technique consists of autonomous solar powered communication systems and involves using the solar cells as an independent power source operating separately from the antennas. A significant disadvantage of this technique is that the solar cells are required to be separated from the antennas by a considerable distance in order to ensure that the cells do not deteriorate the RF characteristics of the antennas. This would suggest that this type of integration is not suitable for low-profile communication systems, such as mobile handsets and WLAN/WiMAX systems in which extremely limited surface area is available for solar combination. The second technique, on the other hand, is the full integration of photovoltaics with microwave antennas into a compact multifunctional communication system, which involves the use of solar cells as a part of RF operation.

In view of this, considerable amount of research has been carried out in the literature on the full integration of solar cells with microwave antennas. In general, work demonstrated in the literature involves the investigation of two types of full solar antenna combination topologies, which can be given as the use of solar cells as an RF ground plane [2, 3] and as an RF radiating element [4, 5], respectively. The drawback of using solar cells as an RF ground plane is that the radiating element, which is conventionally opaque in structure, is placed upon the solar cell and therefore shading the cell and reducing the solar efficiency of the antenna. This has been addressed in [6, 7] and [8] where optical transparency of the radiating patch element has been increased by meshing the patch and making the patch from a transparent conductive material, AgHT-4, respectively. However, special printing equipment is required to be able to apply the meshing technique while the cost of transparent conductive materials is expensive.

A significant drawback to the second solar antenna combination topology, which is the use of solar cells as an RF radiating element, is that this technique cannot be applied for multiband/wideband applications where modification in the traditional patch geometry, such as capacitive slot-loading [9, 10], is required. This is due to the requirement of the solar cells operating as an RF radiating element to be homogeneous in structure for an optimum solar performance.

In this paper, a novel self-complementary shaped multiple-L slot loaded suspended microstrip patch antenna stacked with a polycrystalline silicon (poly-Si) solar cell operating as an RF parasitic patch element is demonstrated for 2.4/5.2 GHz band WLAN and 2.5/3.3/5.8 GHz band WiMAX networks. In addition to providing a full coverage at the frequency bands required for these networks,

the proposed solar antenna uses a stacked solar antenna combination topology, addressing the drawbacks of the existing solar antenna combination topologies studied in the literature by enabling the patch to be modified for multiband operation and the stacked cell to operate without being shaded by any RF components of the antenna ensuring an optimum solar efficiency.

2. SLOT-LOADED STACKED SOLAR PATCH ANTENNA DESIGN

Microstrip patch antennas have various advantages, such as their compact planar geometries making them easily mountable on planar surfaces and low-cost manufacturing, which make them a suitable candidate to be employed in low-profile WLAN and WiMAX systems. However, typical narrow impedance bandwidth performance of conventional microstrip patch antennas brings a significant challenge limiting the usability of these antennas when it comes to multiband/wideband applications. To this end, considerable amount of research has been conducted in the literature in order to enhance the resonance characteristics of microstrip patch antennas including capacitive slot-loaded microstrip patch antennas [9, 10], stacked microstrip patch antennas [11–13] and suspended microstrip patch antennas [14–16].

The solar patch antenna proposed in this paper applies these techniques by introducing a slot loaded microstrip patch printed on a suspended substrate stacked with a poly-Si solar cell as demonstrated in Figure 1.

As illustrated in Figure 1, the modified patch together with the microstrip feed line has been printed on a low-loss RT/Duroid 5870 substrate, $\varepsilon_r = 2.33$ and $\tan\delta = 0.0012$, which has been suspended at 6 mm above the ground plane. The modified microstrip patch has been loaded with self-complementary shaped multiple-L slots responsible for modifying the current paths of multiple TM_{mn} propagation modes as demonstrated in this paper. The microstrip patch has been stacked with a poly-Si solar cell suspended at 3 mm above the patch as illustrated in Figure 1(b). In order to withdraw the current produced by the poly-Si solar cell to a DC load connected to the cell terminals, as shown in Figure 1(b) and Figure 1(c) copper wires with a diameter of 0.8 mm have been connected to the positive and negative terminals of the poly-Si solar cell whose detailed structure is given in Figure 2. It should be noted here that the terminals of the stacked solar cell have been terminated in a DC load impedance of 220 Ω representing a conventional DC termination of a solar cell at the maximum power

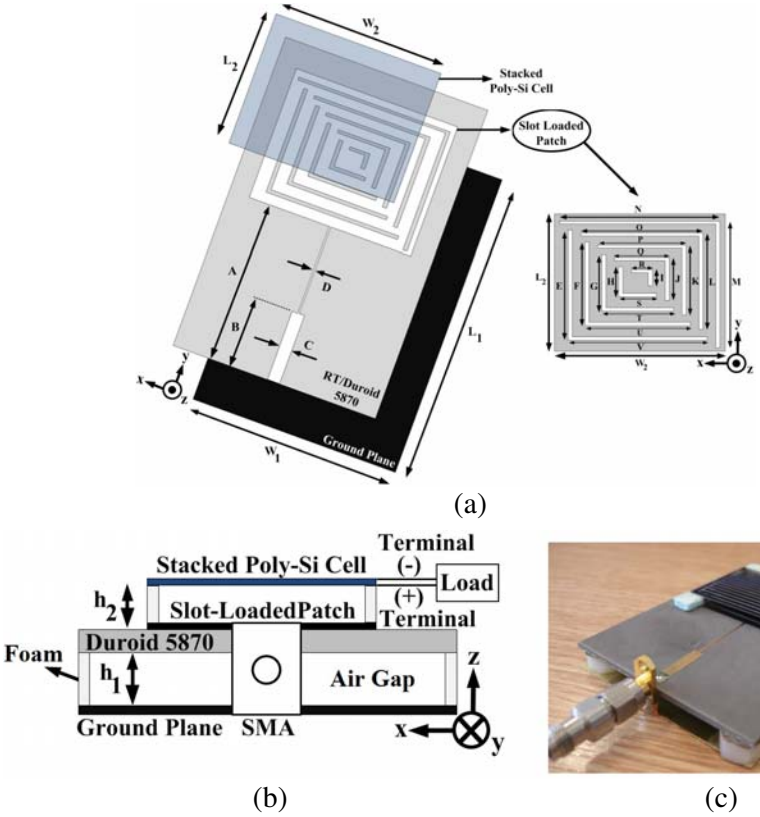

Figure 1. Fabricated solar patch antenna. (a) Top view, (b) back view, (c) overall view. Dimensions (in mm): $A = 41.5$, $B = 18.3$, $C = 3.2$, $D = 0.38$, $E = 27.8$, $F = 21.1$, $G = 14.4$, $H = 7.6$, $I = 4.1$, $J = 10.8$, $K = 17.6$, $L = 24.3$, $M = 32$, $N = 40.5$, $O = 30.9$, $P = 22.3$, $Q = 13.8$, $R = 5.3$, $S = 9.5$, $T = 18.1$, $U = 26.6$, $V = 35.1$, $W_1 = 60$, $W_2 = 43$, $L_1 = 90$, $L_2 = 33$, $h_1 = 6$, $h_2 = 3$, L-slot width = 1.

point.

As can be seen in Figure 2, the poly-Si solar cell consists of two metal contacts, a top grid (negative DC terminal) and a bottom solid (positive DC terminal), respectively, together with a silicon layer in between. From an RF point of view, attention should be given to the bottom metal contact of the cell, which is homogeneous in structure allowing the cell to be used as a suspended RF stacked parasitic patch element in addition to its photovoltaic function which is to generate DC power output to power the communication system in which the

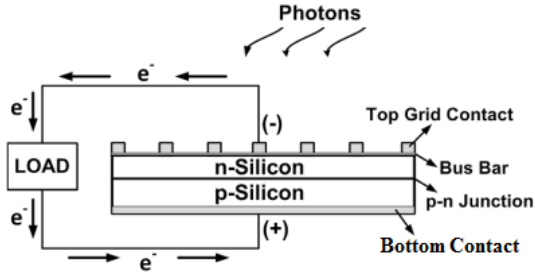

Figure 2. Structure of the stacked poly-Si solar cell.

proposed solar antenna can be built. A significant challenge that needs to be addressed here is the requirement of the effect of the DC copper wires at the cell terminals on the RF antenna performance to be minimized. As illustrated in this paper, this has been achieved by connecting the DC load to the terminals of the stacked poly-Si solar cell at the non-radiating edge.

3. SIMULATION AND MEASUREMENT RESULTS

The simulated and measured reflection coefficient (S_{11}) patterns are demonstrated in Figure 3. The S_{11} simulations have been performed in CST Microwave Studio while the measurements have been taken using an E8364B vector network analyzer (VNA).

As can be seen in Figure 3, there is good agreement between the simulated and measured S_{11} patterns. In order to determine the equivalent TM_{mn} propagation modes introduced by

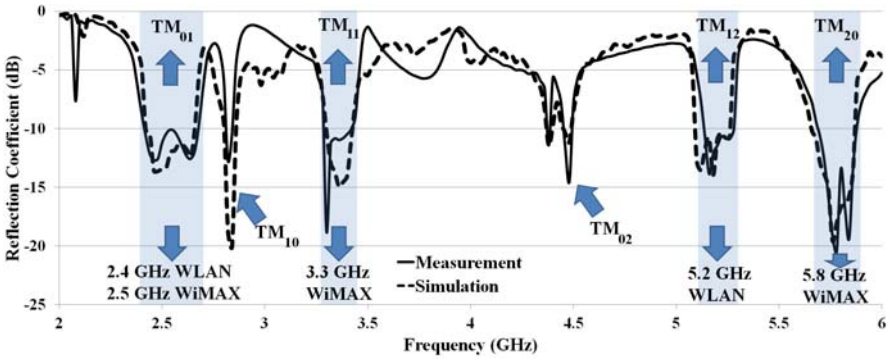

Figure 3. Simulated and measured S_{11} patterns.

the self-complementary shaped multiple-L slot loading regarding the operational frequency bands demonstrated in Figure 3, Equation (1) given below has been used [17]. In Equation (1), L_{eff} and W_{eff} represent the effective patch length and width determined by the L-slots modifying the surface current paths of the supported TM_{mn} modes while ε_{reff} and c are the effective substrate dielectric constant and the speed of light, respectively.

$$f_{mn} = \frac{c}{2\sqrt{\varepsilon_{reff}}}\sqrt{\left(\frac{m}{L_{eff}}\right)^2 + \left(\frac{n}{W_{eff}}\right)^2} \quad (1)$$

Supporting the propagation modes TM_{01}, TM_{10}, TM_{11}, TM_{02}, TM_{12} and TM_{20} across the investigated frequency band of 2–6 GHz as given in Figure 3, the proposed solar patch antenna operates at the measured frequency bands of 2.4–2.71 GHz, 3.29–3.44 GHz, 5.14–5.35 GHz, and 5.68–5.88 GHz, respectively, fully covering the frequency bands required for 2.4/5.2 GHz band WLAN (2.4–2.484 GHz/5.15–5.35 GHz) and 2.5/3.3/5.8 GHz band WiMAX (2.5–2.7 GHz/3.3–3.4 GHz/5.725–5.825 GHz) networks. The S_{11} performance of the proposed solar patch antenna is summarized in Table 1.

Table 1. Measured S_{11} performance of the proposed solar patch antenna.

Resonance	Frequency Band	BW (%)	Covered Networks	Propagation Mode
1	2.4–2.71	12.4	2.4 GHz WLAN 2.5 GHz WiMAX	TM_{01}
2	3.29–3.44	4.5	3.3 GHz WiMAX	TM_{11}
3	5.14–5.35	4	5.2 GHz WLAN	TM_{12}
4	5.68–5.88	3.5	5.8 GHz WiMAX	TM_{20}

The simulated current distributions across the surface of the proposed multiple-L slot loaded suspended patch at the frequencies of 2.5, 3.3, 5.2 and 5.8 GHz are shown in Figure 4.

As can be seen in Figure 4, the introduced self-complementary shaped multiple-L slots modify the current path across the patch surface. Whereas the slots at the patch center play a significant role in the determination of the current paths of TM_{01}, TM_{10} and TM_{11} propagation modes, the slots close to the edges have a considerable effect on shaping the current paths of TM_{02}, TM_{12} and TM_{20} propagation modes.

The E-plane and H-plane far-field radiation pattern measurements have been carried out in an anechoic chamber with an input

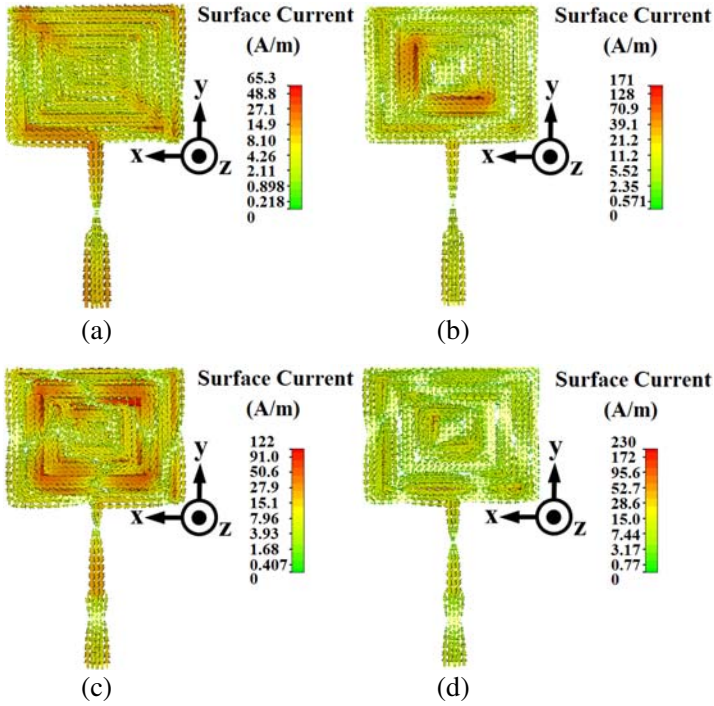

Figure 4. Simulated current distributions across the slot loaded suspended microstrip patch together with the feed line taken at (a) 2.5 GHz, (b) 3.3 GHz, (c) 5.2 GHz, (d) 5.8 GHz.

Table 2. Measured radiation performance of the proposed solar patch antenna.

Frequency (GHz)	Measured Gain (dBi)	Total Radiation Efficiency (%)
2.5	8.49	87.7
3.3	7.11	82
5.2	9.4	81.6
5.8	8.48	81.4

power level of 14 dBm. For the measurements, a circularly-polarized conical spiral antenna with a gain of 4 dBi has been used as a reference antenna. The measured E-plane and H-plane far-field radiation patterns are demonstrated in Figure 5 together with the radiation efficiency and gain values given in Table 2.

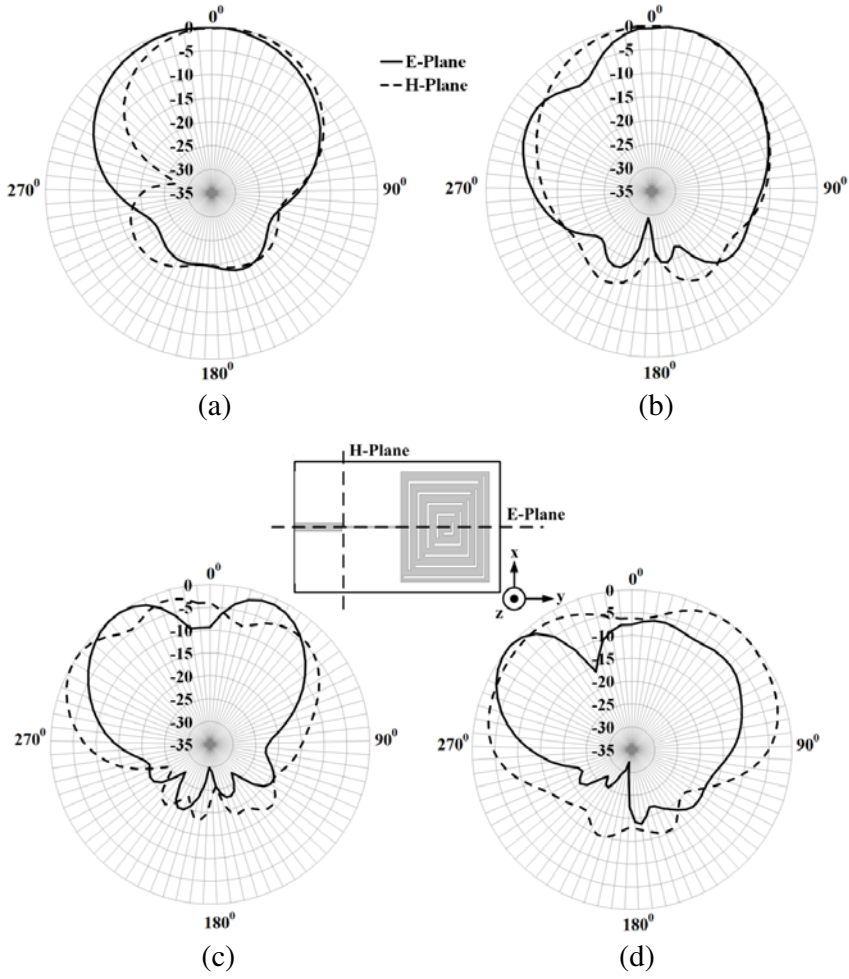

Figure 5. Measured E-plane and H-plane far-field radiation patterns at (a) 2.5 GHz, (b) 3.3 GHz, (c) 5.2 GHz, (d) 5.8 GHz.

As expected from TM_{01} mode, the radiation is in broadside direction at 2.5 GHz as demonstrated in Figure 5(a). For TM_{11} mode at 3.3 GHz, broadside radiation is still present as illustrated in Figure 5(b) replacing the conical off-broadside pattern of conventional rectangular mictostrip patch antennas operating at TM_{11} mode [18]. This is due to the modified current distribution along the width and the length of the proposed slot-loaded patch. If attention is given to Figure 5(c), separation in broadside radiation in E-plane

can clearly be seen enabling the proposed antenna to be used in multipath applications at this frequency. This separation is due to the nature of TM_{12}, which ideally introduces a null in the broadside direction. Similarly, at 5.8 GHz illustrated in Figure 5(d), multipath conical radiation pattern with a separation in near-broadside direction is present introduced by the propagation mode TM_{20}. As given in Table 2, the proposed solar patch antenna demonstrates an adequate gain performance with relatively high measured gains in comparison to traditional gain performance of conventional microstrip patch antennas due to the presence of the stacked poly-Si solar cell operating as a parasitic patch element in the proposed design which also contributes to the radiation as a second radiator.

In this paper, the effect of solar combination on the RF antenna performance has also been studied by investigating the S_{11} responses of the proposed patch antenna with/without the stacked poly-Si solar cell, and the effect of DC wires connected to the terminals of the cell on the RF response of the antenna. In view of this, firstly, S_{11} measurements of the proposed antenna have been taken with and without the stacked poly-Si solar cell and a comparison between the obtained results is made in Figure 6.

As can be seen in Figure 6, the multiband frequency response is present regardless of the presence of the stacked poly-Si solar cell as a result of the proposed complementary shaped multiple-L slot loaded suspended patch structure. However, the proposed poly-Si solar cell stacked geometry brings a considerable enhancement at the resonance bands enabling the antenna to provide a full coverage for

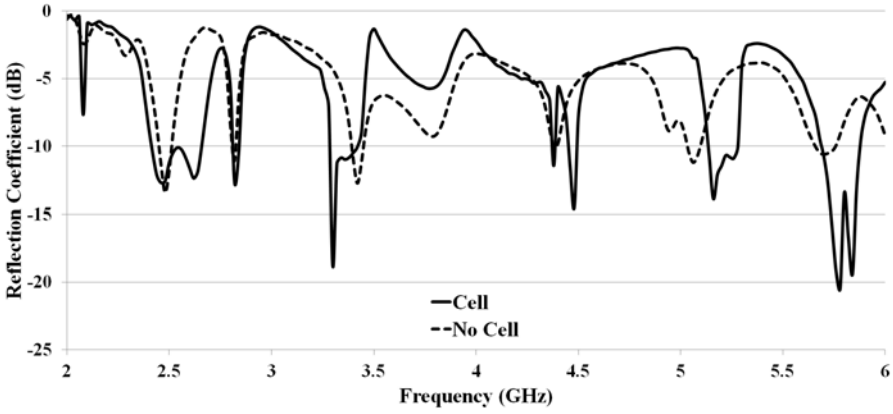

Figure 6. Measured S_{11} patterns with and without the stacked poly-Si solar cell.

2.4/5.2 GHz band WLAN and 2.5/3.3/5.8 GHz band WiMAX networks in comparison to the microstrip patch without the stacked cell.

Secondly, the effect of DC wires connected to the terminals of the stacked poly-Si solar cell as shown in Figure 1(b) has been investigated by measuring the S_{11} responses of the solar patch antenna with and without the DC connections terminated in 220 Ω DC load.

In Figure 7, the difference between the S_{11} responses of the solar patch antenna with and without the DC connections is negligible when the DC wires are connected to the terminals of the stacked cell at the non-radiating edge (x-z plane) as proposed in this paper. Connecting these wires to the terminals of the cell at the radiating edge (y-z plane), however, results in a considerable deterioration in the S_{11} response of the antenna especially at 3.3 GHz and 5.8 GHz resonance bands where −10 dB impedance bandwidth is narrower by 75% and 40%, respectively, in comparison to the proposed non-radiating edge wire connected design. This is due to the surface current across the bottom contact of the stacked cell, which is induced by the L-slot loaded patch, to continue to flow through the DC wires resulting in them being a part of the RF operation and acting as a deteriorating unwanted radiator at the radiating edge.

Solar measurements have been taken in a solar simulator providing a homogeneous illumination intensity of 1000 W/m^2. The antenna design made it not possible to measure I-V at standard temperature, all data have been measured at 32 ± 3°C. Open-circuit voltage and short-circuit current have been measured as 0.57 V and 563.8 mA with a solar efficiency of 10%.

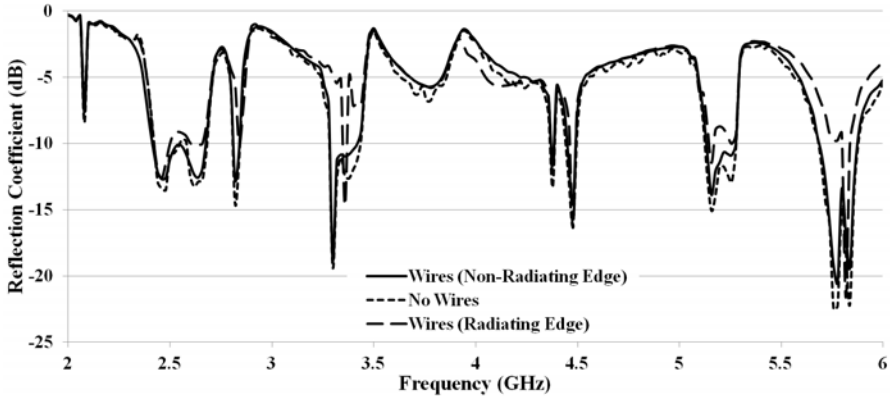

Figure 7. Measured S_{11} patterns with and without DC wires connected to the terminals of the stacked poly-Si solar cell.

4. CONCLUSION

A poly-Si solar cell stacked self-complementary shaped multiple-L slot loaded suspended microstrip patch antenna has been demonstrated for 2.4/5.2 GHz band WLAN and 2.5/3.3/5.8 GHz band WiMAX networks. The proposed solar patch antenna operates at the measured frequency bands of 2.4–2.71 GHz, 3.29–3.44 GHz, 5.14–5.35 GHz and 5.68–5.88 GHz covering the required frequency bands for the networks mentioned above in full with measured gains of 8.49 dBi, 7.11 dBi, 9.4 dBi and 8.48 dBi, respectively. In addition to working as an RF parasitic patch element, the poly-Si solar cell operates with an adequate 10% solar efficiency achieved as a result of the proposed stacked solar antenna combination topology. The measured S_{11} and gain characteristics with the adequate solar performance confirm the suitability of the proposed solar patch antenna for low-profile multifunctional WLAN and WiMAX systems.

REFERENCES

1. Todd, T. D., A. A. Sayegh, M. N. Smadi, and D. Zhao, "The need for access point power saving in solar powered WLAN mesh networks," *IEEE Network*, Vol. 22, No. 3, 4–10, May 2008.
2. Shynu, S. V., M. J. R. Ons, P. McEvoy, M. J. Ammann, S. J. McCormack, and B. Norton, "Integration of microstrip patch antenna with polycrystalline silicon solar cell," *IEEE Trans. Antennas Propag.*, Vol. 57, No. 12, 3969–3972, Dec. 2009.
3. Shynu, S. V., M. J. Ammann, and B. Norton, "Quarter-wave metal plate solar antenna," *Electron. Lett.*, Vol. 44, No. 9, 570–571, Apr. 2008.
4. Danesh, M. and J. R. Long, "An autonomous wireless sensor node incorporating a solar cell antenna for energy harvesting," *IEEE Trans. Microw. Theory Tech.*, Vol. 59, No. 12, 3546–3555, Nov. 2011.
5. Vaccaro, S., J. R. Mosig, and P. de Maagt, "Making planar antennas out of solar cells," *Electron. Lett.*, Vol. 38, No. 17, 945–947, Aug. 2002.
6. Turpin, T. W. and R. Baktur, "Meshed patch antennas integrated on solar cells," *IEEE Antennas Wireless Propag. Lett.*, Vol. 8, 693–696, 2009.
7. Yurduseven, O., D. Smith, and M. Elsdon, "UWB meshed solar monopole antenna," *Electron. Lett.*, Vol. 49, No. 9, 582–584, Apr. 2013.

8. Roo-Ons, M. J., S. V. Shynu, M. J. Ammann, S. J. McCormack, and B. Norton, "Transparent patch antenna on a-Si thin-film glass solar module," *Electron. Lett.*, Vol. 47, No. 2, 85–86, Jan. 2011.
9. Vegni, C. and F. Bilotti, "Parametric analysis of slot-loaded trapezoidal patch antennas," *IEEE Trans. Antennas Propag.*, Vol. 50, No. 9, 1291–1298, Sep. 2002.
10. Krishna, D. D., M. Gopikrishna, C. K. Aanandan, P. Mohanan, and K. Vasudevan, "Compact dual band slot loaded circular microstrip antenna with a superstrate," *Progress In Electromagnetics Research*, Vol. 83, 245–255, 2008.
11. Fortaki, T., L. Djouane, F. Chebara, and A. Benghalia, "On the dual-frequency behavior of stacked microstrip patches," *IEEE Antennas Wireless Propag. Lett.*, Vol. 7, 310–313, 2008.
12. Ansari, J. A. and R. B. Ram, "Broadband stacked U-slot microstrip patch antenna," *Progress In Electromagnetics Research Letters*, Vol. 4, 17–24, 2008.
13. Anguera, J., C. Puente, and C. Borja, "Dual frequency broadband microstrip antenna with a reactive loading and stacked elements," *Progress In Electromagnetics Research Letters*, Vol. 10, 1–10, 2009.
14. Gardelli, R., G. La Cono, and M. Albani, "A low-cost suspended patch antenna for WLAN access points and point-to-point link," *IEEE Antennas Wireless Propag. Lett.*, Vol. 3, No. 1, 90–93, Dec. 2004.
15. Kasabegoudar, V. G. and K. J. Vinoy, "A broadband suspended microstrip antenna for circular polarization," *Progress In Electromagnetics Research*, Vol. 90, 353–368, 2009.
16. Deng, J.-Y., L.-X. Guo, T.-Q. Fan, Z.-S. Wu, Y.-J. Hu, and J. H. Yang, "Wideband circularly polarized suspended patch antenna with indented edge and gap-coupled feed," *Progress In Electromagnetics Research*, Vol. 135, 151–159, 2013.
17. Deshmukh, A. A. and K. P. Ray, "Analysis of broadband Psi (ψ)-shaped microstrip antennas," *IEEE Antennas Propag. Mag.*, Vol. 55, No. 2, 107–123, Apr. 2013.
18. Lee, K. F. and K. M. Luk, *Microstrip Patch Antennas*, Imperial College Press, 2011.